Boundary Extraction Enhanced Inverse Scattering Method for Microwave Mammography

Kazuki Noritake and Shouhei Kidera,
Graduate School of Informatics and Engineering, University of Electro-Communications, Japan
noritake.kazuki@ems.cei.uec.ac.jp, kidera@uec.ac.jp

***Abstract*—Microwave mammography is a promising alternative from the X-ray based imaging modality, in terms of compactness, low cost and cell-friendly exposure. This paper focuses on the accuracy enhancement by incorporating breast surface boundary extraction into the inverse scattering analysis algorithm, known as distorted born iterative method (DBIM). Many studies have reported that the reconstruction accuracy of the DBIM or other inverse scattering algorithms largely depends on an initial estimate of boundary surrounding object, namely, skin surface shape of breast media. The Envelope method achieves highly accurate boundary extraction by processing a group of reflection time-delays. The accuracy of boundary extraction of Envelope depends on that of time-delay estimation, which is mostly processed by the filter based on waveform matching between observed and reference signals. However, the coupling effect between an antenna and a breast surface deforms an observed waveforms from reference one. To mitigate this problem, this paper introduces the finite-difference time-domain (FDTD) -based waveform correction for more accurate boundary extraction. Numerical simulations based on realistic breast phantoms derived from magnetic resonance imaging (MRI) demonstrate that the proposed method significantly enhances the accuracy for the DBIM based reconstruction of dielectric profile in highly heterogeneous case.**

***Index Terms*—Microwave mammography, Distorted born iterative method (DBIM), Envelope-based boundary extraction, FDTD-based waveform correction.**

I. Introduction

According to the world cancer research fund (WCRF), the breast cancer is the most widely diagnosed cancer in women. Although the X-ray mammography is the most prevailed screening technique for the detection of malignant tumors, there is a potential risk for harming the cells and involving measurements of the human breast under high compression; this incurs a lower examination rates, especially in young women. As an alternative screening tool, microwave mammography offers several advantages *e.g.* portability, non-contact and cell-friendly measurement, and low cost for the equipment.

A number of studies have investigated a significant contrast between the dielectric properties of normal tissues (adipose dominant) and malignant tumors[1]. This electric contrast is the physical basis of microwave mammography. Various imaging algorithms have been developed for cancer detection or characterization, the methods of which are divided into two categories. One is a confocal algorithm, *e.g.* beamforming[2] and the other is an inverse scattering algorithm, *e.g.* diffraction tomography, Born approximation or distorted Born iterative method (DBIM)[3]. This paper focuses on the DBIM algorithm, which is one of the most promising inverse scattering algorithm, for reconstruction of the unknown dielectric profile of a object area from measured scattered field data. Many reports have revealed that the DBIM-based algorithm faces the problem as to severe sensitivity to an initial estimate of dielectric property map or outer skin boundary[4][5]. A number of breast surface shape estimation methods have been developed[6], most of which are based on the Envelope method[7]. It has been reported that the reconstruction accuracy for boundary extraction by the Envelope method largely depends on the accuracy for range estimation from the antennae to the breast surface. However, due to the coupling effect between antenna and skin surface, a skin reflection waveform often mismatches the reference one, which leads an error for range estimation based on waveform matching based filter, *e.g.* matched filter.

To address with the above issue, this paper proposes a direct compensation scheme for breast boundary estimation using FDTD recovered signal. The range error can be directly compensated by assessing the time-shift between the observed and FDTD recovered signal, where a near-field effect should be considered. Finally, the proposed method incorporates the above accuracy enhanced Envelope method into the DBIM process. The result of FDTD-based numerical simulation using MRI-derived realistic numerical phantoms demonstrate that the proposed algorithm considerably enhances the convergence speed and reconstruction accuracy of the DBIM outputs for highly heterogeneous breast media.

II. Observation model

Figure 1 shows the observation model. Multiple transmitters and receivers array are located along the circumference curve, which surrounds an object area. The breast medium is comprised of skin, adipose, and fibro-glandular tissues, each of which have a lossy, dispersive, and isotropic dielectric propertie. $E^{\rm obs}(\boldsymbol{r}_{\rm t}, \boldsymbol{r}_{\rm r}; t)$ denotes the observed scattered electric field at the time t, where $\boldsymbol{r}_{\rm t}$ and $\boldsymbol{r}_{\rm r}$ denote the locations of transmitter and receiver, respectively.

III. Proposed Inverse Scattering Algorithm

A. Distorted Born Iterative Method (DBIM)

The dielectric profile in breast media can be reconstructed via solving the Helmholtz type integral equation[8]. Here,

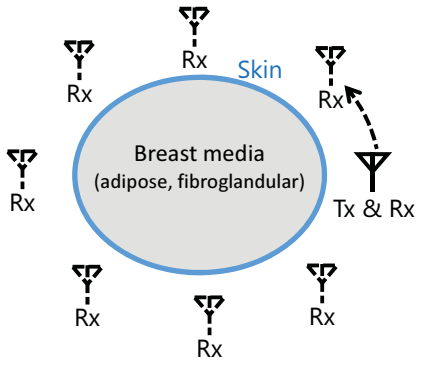

Fig. 1: Observation model.

focusing on the scattered field $E^{\mathrm{scat}}(\boldsymbol{r})$, which is observed at the location $\boldsymbol{r}$, the following integral equation holds:

$$E^{\mathrm{scat}}(\boldsymbol{r}) \equiv E^{\mathrm{total}}(\boldsymbol{r}) - E^{\mathrm{in}}(\boldsymbol{r}) = \omega^2 \mu \int_V G_0(\boldsymbol{r}, \boldsymbol{r}') E^{\mathrm{total}}(\boldsymbol{r}') o(\boldsymbol{r}') d\boldsymbol{r}' \quad (1)$$

where V is object area, $E^{\mathrm{scat}}(\boldsymbol{r})$ and $E^{\mathrm{total}}(\boldsymbol{r})$ are the scattered and total electric fields, respectively, and $E^{\mathrm{in}}(\boldsymbol{r})$ is the incident field in the presence of the background complex relative permittivity denoted as $\epsilon_0(\boldsymbol{r})$, $G_0(\boldsymbol{r}, \boldsymbol{r}')$ is the Green's function assuming the background media, and $o(\boldsymbol{r}) = \epsilon(\boldsymbol{r}) - \epsilon_0(\boldsymbol{r})$ denotes the object function, where $\epsilon(\boldsymbol{r})$ is an actual complex relative permittivity. The inverse scattering algorithm solves the object function $o(\boldsymbol{r})$ using the recorded scattered field $E^{\mathrm{scat}}(\boldsymbol{r})$. The difference between the true and assumed (or estimated) background media of the total field as $\Delta E^{\mathrm{total}}$ is formulated as:

$$\Delta E^{\mathrm{total}}(\boldsymbol{r}) = E^{\mathrm{total}}(\boldsymbol{r}) - E_{\mathrm{b}}^{\mathrm{total}}(\boldsymbol{r}) = \omega^2 \mu \int_V G_{\mathrm{b}}(\boldsymbol{r}, \boldsymbol{r}') E^{\mathrm{total}}(\boldsymbol{r}) \Delta o(\boldsymbol{r}') d\boldsymbol{r}' \quad (2)$$

where $G_{\mathrm{b}}(\boldsymbol{r}, \boldsymbol{r}')$ is the Green's function of the background medium, $\Delta o(\boldsymbol{r}) = o(\boldsymbol{r}) - o_{\mathrm{b}}(\boldsymbol{r})$ and $o_{\mathrm{b}}(\boldsymbol{r})$ is the object function of background. Here, assuming that $\Delta o(\boldsymbol{r})$ is sufficiently small, $E^{\mathrm{total}}(\boldsymbol{r}) \simeq E_{\mathrm{b}}^{\mathrm{total}}(\boldsymbol{r})$ holds, and Eq. (2) is approximated as:

$$\Delta E^{\mathrm{total}}(\boldsymbol{r}) \simeq \omega^2 \mu \int_V G_{\mathrm{b}}(\boldsymbol{r}, \boldsymbol{r}') E_{\mathrm{b}}^{\mathrm{total}}(\boldsymbol{r}) \Delta o(\boldsymbol{r}') d\boldsymbol{r}'. \quad (3)$$

The DBIM sequentially updates $o_{\mathrm{b}}(\boldsymbol{r})$, $G_{\mathrm{b}}(\boldsymbol{r}, \boldsymbol{r}')$ and $E_{\mathrm{b}}^{\mathrm{total}}(\boldsymbol{r})$ in order to minimize $|\Delta E^{\mathrm{total}}(\boldsymbol{r})|^2$. In the case of dispersive media, such as breast, each parameter in the assumed dispersive model (*e.g.* Debye model) is updated using multiple frequency data[3][9].

While a number of literature revealed that the DBIM reconstructs accurate dielectric map even in highly heterogeneous case, the iterative procedure requires an accurate estimate of initial dielectric profile and an outer boundary of an object area. The accuracy of such prior estimation significantly affects the final output of the DBIM.

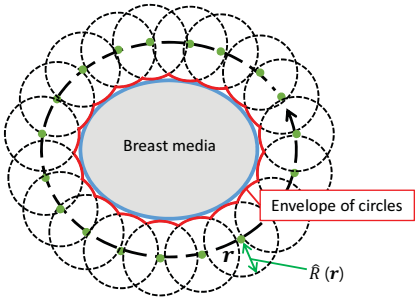

Fig. 2: Envelope based boundary reconstruction scheme.

B. Accuracy enhanced boundary extraction incorporating Envelope and FDTD recovery signal

To address with the above mentioned drawback in the DBIM method, we introduce the Envelope based boundary extraction method [7]. This method is based on a simple principle that an object's outer boundary can be expressed as an envelope of circles (or ellipsoid in bi-static case) with the center as the antenna location and the radius as the measured range between the antenna and skin surface. Figure 2 shows the principle of envelope-based surface extraction, assuming the mono-static, namely, $\boldsymbol{r}_{\mathrm{t}} = \boldsymbol{r}_{\mathrm{r}}$. Here, the range measured at the antenna location $(\boldsymbol{r}_{\mathrm{t}}, \boldsymbol{r}_{\mathrm{r}})$ is defined as $\hat{R}(\boldsymbol{r}_{\mathrm{t}}, \boldsymbol{r}_{\mathrm{r}})$. $\hat{R}(\boldsymbol{r})$ can be extracted from the local maximum of the output of the filter (*e.g.* matched filter) using a specific reference signal $E^{\mathrm{ref}}(t)$. It is obvious that the shape estimation by the Envelope method relies on accurate range extraction as $\hat{R}(\boldsymbol{r}_{\mathrm{t}}, \boldsymbol{r}_{\mathrm{r}})$. The accuracy of range extraction depends on the waveform similarity between the observed and the assumed reference signals. However, in most case, the antennae and breast surface are closely located within the central wavelength of the transmitted pulse. Thus, in such the near-field observation, a observed waveform is considerably deformed from the assumed reference one due to a coupling effect.

To enhance the accuracy of breast surface estimation, this paper introduces a direct range compensation using the FDTD-recovered waveform. In this method, the reference signal is updated by the FDTD-based forward solver with a prior estimation of skin surface derived from the Envelope method. Since the FDTD-recovered signal denoted as $\tilde{E}^{\mathrm{obs}}(\boldsymbol{r}_{\mathrm{t}}, \boldsymbol{r}_r; t)$, includes the coupling effect between the skin and antennae, it is predicted that it upgrades the accuracy in range estimation by compensating the above mentioned waveform mismatch. This method directly updates the range as;

$$\tilde{R}(\boldsymbol{r}_{\mathrm{t}}, \boldsymbol{r}_{\mathrm{r}}) = \hat{R}(\boldsymbol{r}_{\mathrm{t}}, \boldsymbol{r}_{\mathrm{r}}) + \mathrm{c}\Delta\tau(\boldsymbol{r}_{\mathrm{t}}, \boldsymbol{r}_{\mathrm{r}})/2, \quad (4)$$

where c is the speed of light in the air, and $\Delta\tau(\boldsymbol{r}_{\mathrm{t}}, \boldsymbol{r}_{\mathrm{r}})$ is calculated as;

$$\Delta\tau(\boldsymbol{r}_{\mathrm{t}}, \boldsymbol{r}_{\mathrm{r}}) = \arg\max_{\tau} [E^{\mathrm{obs}}(\boldsymbol{r}_{\mathrm{t}}, \boldsymbol{r}_{\mathrm{r}}; t) \star \tilde{E}^{\mathrm{obs}}(\boldsymbol{r}_{\mathrm{t}}, \boldsymbol{r}_{\mathrm{r}}; t)](\tau), \quad (5)$$

where $\star$ denotes the operator of cross-correlation. The boundary of the breast surface is also updated by the Envelope method using the group of $\tilde{R}(\boldsymbol{r}_{\mathrm{t}}, \boldsymbol{r}_{\mathrm{r}})$.

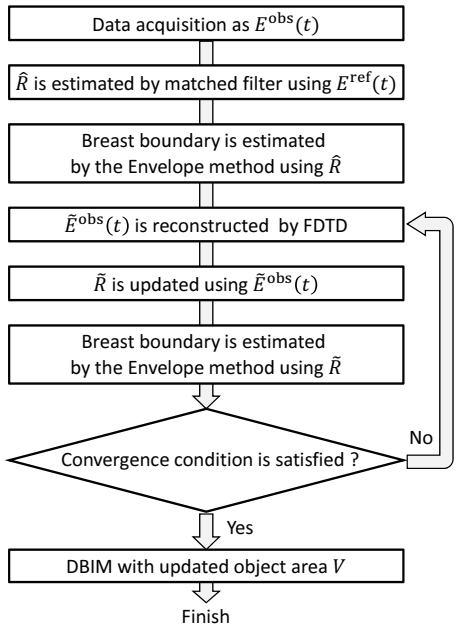

Fig. 3: Flowchart of the proposed method.

C. Incorporation DBIM and Envelope based Boundary Extraction

Finally, this method incorporates the accuracy enhanced Envelope method and the DBIM as follows.

Step 1) Observation data as $E^{\mathrm{obs}}(\boldsymbol{r}_{\mathrm{t}}, \boldsymbol{r}_{\mathrm{r}}; t)$ are recorded at each combination of $\boldsymbol{r}_{\mathrm{t}}$ and $\boldsymbol{r}_{\mathrm{r}}$, which is retrieved by the difference of total fields with and without object.

Step 2) Initial boundary shape is estimated by the Envelope method.

Step 3) Reference signal is updated using the FDTD method assuming a prior estimate of dielectric profile and breast boundary in Step 2).

Step 4) Range is compensated in Eq. (4) using FDTD recovered signal.

Step 5) Boundary shape is updated using compensated ranges.

Step 6) Repeating the Step 2) to 5) by the fixed iteration number.

Step 7) Dielectric property assuming single-pole Debye model is reconstructed by DBIM, where object area is determined by the Step 6).

IV. Result in Numerical Test

This section describes the numerical test using simulated array measurements of realistic breast phantoms derived from MRI scans of healthy women [10]: Class 3 (Heterogeneously Dense) phantom and Class 4 (Very Dense) phantom. Figure 4 illustrates the maps of the Debye parameters, ϵ_∞, $\Delta\epsilon$ and σ_s in Class 3 and 4. The transmitting signal formed a raised-cosine modulated pulse with a central frequency is 2.45 GHz, and a bandwidth is 2.7 GHz. The number of arrays is 15, and all combination data as to transmitting and receiving

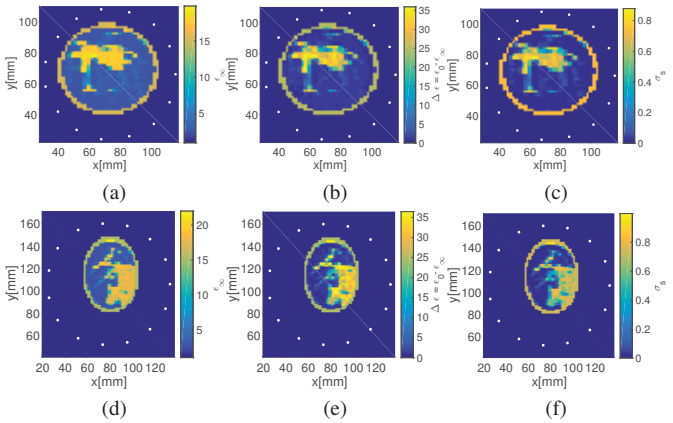

Fig. 4: Maps of the Debye parameter: (a): $\epsilon_\infty(\boldsymbol{r})$, (b) $\Delta\epsilon(\boldsymbol{r})$ and (c) $\sigma_s(\boldsymbol{r})$ in Class 3 phantom. (d): $\epsilon_\infty(\boldsymbol{r})$, (e) $\Delta\epsilon(\boldsymbol{r})$ and (f) $\sigma_s(\boldsymbol{r})$ in Class 4 phantom.

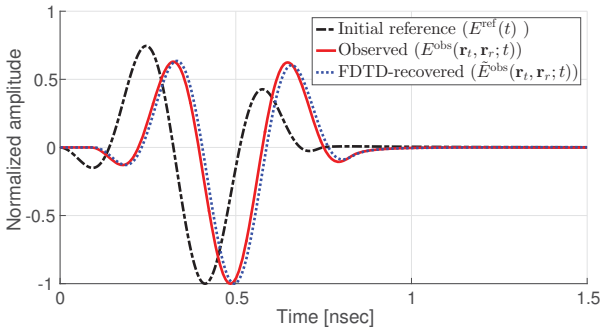

Fig. 5: Waveform comparison among observed signal $E^{\mathrm{obs}}(\boldsymbol{r}_{\mathrm{t}}, \boldsymbol{r}_{\mathrm{r}}; t)$, initial reference signal and FDTD-recovered signal $\tilde{E}^{\mathrm{obs}}(\boldsymbol{r}_{\mathrm{t}}, \boldsymbol{r}_{\mathrm{r}}; t)$.

antennae are processed in the DBIM. The frequency-dependent complex permittivities for the breast phantoms were modeled using the single-pole Debye modelsmodel, which has been demonstrated in its accuracy for a number of real breast specimens [1]. The scattered electric field is calculated by the FDTD method with single-pole Debye model (in-house code provided by the cross-disciplinary electromagnetics laboratory at the University of Wisconsin, Madison). TM (Transverse Magnetic) mode wave is assumed in the two-dimensional problem. Each cell size in FDTD is 2mm. The conjugate gradient for least-squares (CGLS) method is used in the DBIM updating, where the maximum iteration number is set to 20.

Figure 5 shows a comparison of waveforms for the observed, the initial reference, and the FDTD-recovered signals at the specific observation point, assuming Class 2 phantom. $\tilde{E}^{\mathrm{obs}}(\boldsymbol{r}_{\mathrm{t}}, \boldsymbol{r}_{\mathrm{r}}; t)$ is a waveform obtained by the FDTD assuming the initial boundary estimated by the Envelop method. Figure 5 demonstrates that a similarity between $E^{\mathrm{obs}}(t)$ and $\tilde{E}^{\mathrm{obs}}(t)$ is remarkably improved compared with that between $E^{\mathrm{obs}}(t)$ and $E^{\mathrm{ref}}(t)$. Table I summarizes the estimation error for boundary

TABLE I: Error of estimated boundary, defined as Err_V, by Envelope method.

	Iteration num. of waveform compensation		
	0	1	2
Class 3	31.0%	11.8%	5.8%
Class 4	21.2%	9.2%	4.3%

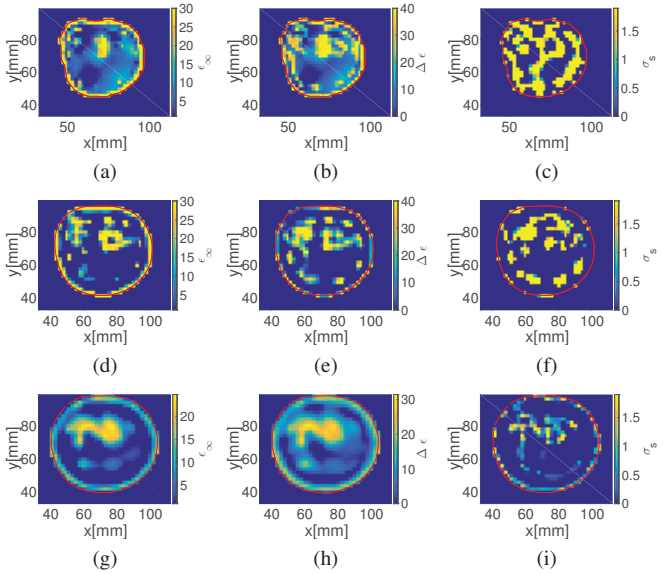

Fig. 6: Reconstruction results of DBIM in Class 3: (a)-(c) :Maps of $\epsilon_\infty(\boldsymbol{r})$, $\Delta\epsilon(\boldsymbol{r})$ and $\sigma_s(\boldsymbol{r})$, where object area is given by the Envelope without range compensation. (d)-(f): Maps of $\epsilon_\infty(\boldsymbol{r})$, $\Delta\epsilon(\boldsymbol{r})$ and $\sigma_s(\boldsymbol{r})$, where object area is given by the Envelope with range compensation (once). (g)-(i): Maps of $\epsilon_\infty(\boldsymbol{r})$, $\Delta\epsilon(\boldsymbol{r})$ and $\sigma_s(\boldsymbol{r})$, where object area is given by the Envelope with range compensation (twice).

estimation of breast media, defined as:

$$\mathrm{Err}_V = \frac{\left|\int_{V_{\mathrm{true}}} dr - \int_{\hat{V}} dr\right|}{\int_{V_{\mathrm{true}}} dr}, \tag{6}$$

where V_{true} and $\hat{V}$ are the areas of object function of the true and estimated by the Envelope, respectively. Table I verifies that our proposed method considerably enhances the accuracy of surface shape estimation in both classes.

Figure 6 and 7 show the reconstruction results of DBIM using the initial object boundary estimated by the Envelope with or without range compensation, at Class 3 and Class 4 phantoms, respectively. These figures demonstrate that the reconstruction accuracy of DBIM largely depends on that of boundary estimation, and the proposed method successfully enhances its accuracy. Here, for the quantitative analysis, the normalized root mean square error (NRME) in the reconstruction for each Debye parameter is defined as

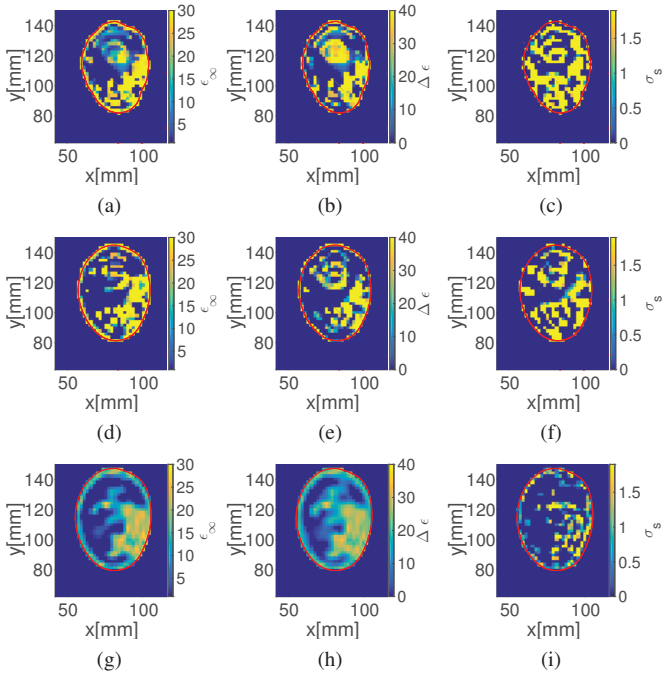

Fig. 7: Reconstruction results of DBIM in Class 4: (a)-(c) :Maps of $\epsilon_\infty(\boldsymbol{r})$, $\Delta\epsilon(\boldsymbol{r})$ and $\sigma_s(\boldsymbol{r})$, where object area is given by the Envelope without range compensation. (d)-(f): Maps of $\epsilon_\infty(\boldsymbol{r})$, $\Delta\epsilon(\boldsymbol{r})$ and $\sigma_s(\boldsymbol{r})$, where object area is given by the Envelope with range compensation (once). (g)-(i): Maps of $\epsilon_\infty(\boldsymbol{r})$, $\Delta\epsilon(\boldsymbol{r})$ and $\sigma_s(\boldsymbol{r})$, where object area is given by the Envelope with range compensation (twice).

$$\mathrm{NRMSE}_{\epsilon_\infty,i} = \sqrt{\frac{1}{K}\sum_{k=1}^{K}\left|\frac{\epsilon_{\infty,i}(\boldsymbol{r}_k) - \epsilon_{\infty,\mathrm{true}}(\boldsymbol{r}_k)}{\bar{\epsilon}_{\infty,\mathrm{true}}}\right|^2}, \tag{7}$$

$$\mathrm{NRMSE}_{\Delta\epsilon,i} = \sqrt{\frac{1}{K}\sum_{k=1}^{K}\left|\frac{\Delta\epsilon_i(\boldsymbol{r}_k) - \Delta\epsilon_{\mathrm{true}}(\boldsymbol{r}_k)}{\bar{\Delta}\epsilon_{\mathrm{true}}}\right|^2}, \tag{8}$$

$$\mathrm{NRMSE}_{\sigma_s,i} = \sqrt{\frac{1}{K}\sum_{k=1}^{K}\left|\frac{\sigma_{s,i}(\boldsymbol{r}_k) - \sigma_{s,\mathrm{true}}(\boldsymbol{r}_k)}{\bar{\sigma}_{s,\mathrm{true}}}\right|^2}, \tag{9}$$

where the subscript "true" denotes the true value, K is the total number of cell in object area and the subscript i denotes the estimation results at the i-th iteration in DBIM. Figure 8 shows the NRMSEs for each parameter in Class 3 and Class 4. These results demonstrate that the accuracy enhanced boundary extraction significantly accelerates the convergence speed. Note that, the reconstruction accuracy for σ_s is relatively worse than other parameters. It is considered that there is a significant difference of magnitude of each parameter.

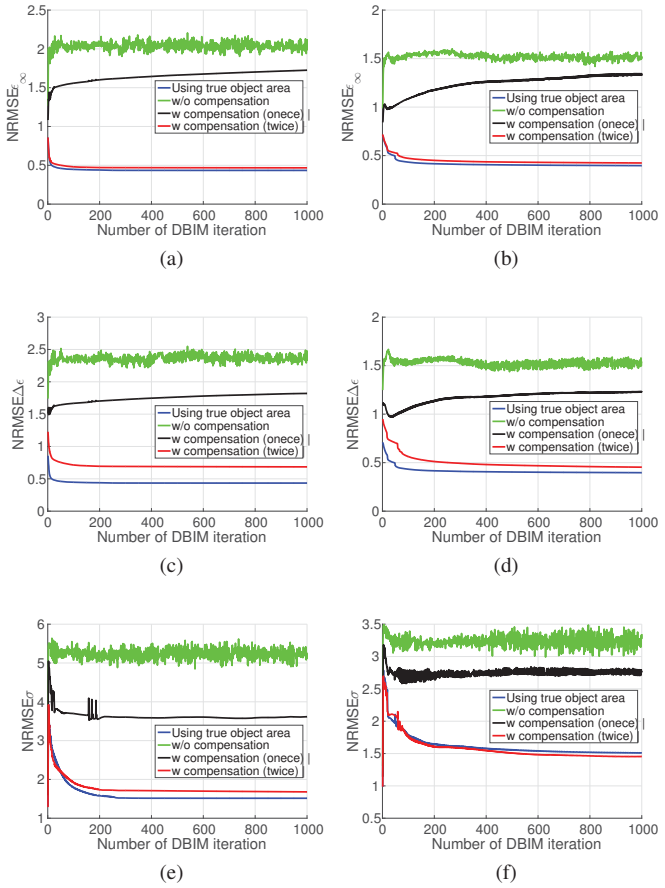

Fig. 8: The NRNSEs for reconstruction of each Debye parameter, (a), (c) and (e) denote $\epsilon_\infty(\boldsymbol{r})$, $\Delta\epsilon(\boldsymbol{r})$ and $\sigma_s(\boldsymbol{r})$ in Class 3 phantom. (b), (d) and (f) denote $\epsilon_\infty(\boldsymbol{r})$, $\Delta\epsilon(\boldsymbol{r})$ and $\sigma_s(\boldsymbol{r})$ in Class 4 phantom.

V. CONCLUSION

This paper introduced the accuracy enhanced boundary extraction method for efficient convergence of DBIM algorithm. The accuracy of Envelope-based boundary extraction can be upgraded by introducing the FDTD-recovered reference signal updating. Numerical test with realistic breast phantoms with highly heterogeneous media, demonstrated that our proposed method considerably enhanced the accuracy and convergence speed of DBIM-based dielectric map reconstruction. It is our future work to investigate this method in the three-dimensional simulation or experimental data.

ACKNOWLEDGMENT

This research and development work was supported by the MIC/SCOPE #162103102.

REFERENCES

[1] M. Lazebnik, D. Popovic, L. McCartney, C. B. Watkins, M. J. Lindstrom, J. Harter, S. Sewall, T. Ogilvie, A. Magliocco, T. M. Breslin, W. Temple, D. Mew, J. H. Booske, M. Okoniewski, and S. C. Hagness, "A large-scale study of the ultrawideband microwave dielectric properties of normal, benign and malignant breast tissues obtained from cancer surgeries", *IOP Publishing Phys. Med. Biol.* vol. 52, pp. 60932093 2007.

[2] E. J. Bond, Xu Li, and S. C. Hagness, "Microwave imaging via space-time beamforming for early detection of breast cancer", *IEEE Trans. Antennas Propagat.*, vol. 1, no. 8, pp. 1690-1705, Aug. 2003.

[3] J. D. Shea, P. Kosmas, S. C. Hagness and B. D. Van Veen., "Three-dimensional microwave imaging of realistic numerical breast phantoms via a multiple-frequency inverse scattering technique", *Am. Assoc. Phys. Med.*, vol. 37, no. 8, pp.4210-4226, Aug.2010.

[4] F. Gao, B. D. Van Veen, and S. C. Hagness, "Sensitivity of the distorted Born iterative method to the initial guess in microwave breast imaging," *IEEE Transactions on Antennas and Propagation*, vol. 63, no. 8, pp. 3540-3547, Aug. 2015.

[5] A. Fhager and M. Persson, "Reconstrunction strategies for microwave imaging of breast; reconstructions constrained to the breast domain", *Microwave Bio Conference (IMBIOC)*, 2017

[6] M. Sarafianou, D.R. Gibbins, I.J. Craddock, M. Klemm, J.A. Leendertz, A. Preece, and R. Benjamin, "Breast Surface Reconstruction Algorithm for a Multi-Static Radar-Based Breast Imaging System", $Proc.4thEur.Conf.AntennasPropag.(EuCAP)$, 2010, pp1-5.

[7] S. Kidera, T. Sakamoto, and T. Sato., "A Robust and Fast Imaging Algorithm with an Envelope of Circles for UWB Pulse Radars", *IEICE Trans Commun*., vol. E90-B, no.7, pp.1801-1809, July.2007.

[8] M. A. Fiddy and R. S. Ritter, 2014, "Introduction to Imaging from Scattered Fields", CRC Prress.

[9] T. J. Cui, W. C. Chew, A. A. Aydiner, and S. Chen,"Inverse Scattering of Two-Dimensional Dielectric Objects Buried in a Lossy Earth Using the Distorted Born Iterative Method", *IEEE Trans. Geosci. Remote Sens.*, vol. 39, no. 2, pp.339-346, Feb.2001.

[10] UWCEM, "Numerical breast phantom repository", URL:https://uwcem.ece.wisc.edu/phantomRepository.html